Article

Development of a Traffic Congestion Prediction and Emergency Lane Development Strategy Based on Object Detection Algorithms

Chaokai Zhang [1,2,3], Hao Cheng [1,*], Rui Wu [1,2], Biyun Ren [1,4], Ye Zhu [3] and Ningbo Peng [2,3,*]

1   College of Mathematics & Physics, Nanjing Tech University, Nanjing 211816, China; 202261228001@njtech.edu.cn (C.Z.); 202261126025@njtech.edu.cn (R.W.); 202261122121@njtech.edu.cn (B.R.)
2   College of Civil Engineering, Nanjing Tech University, Nanjing 211816, China
3   Faculty of Architecture and Civil Engineering, Huaiyin Institute of Technology, Huaian 223001, China; zhuye1986@hyit.edu.cn
4   School of Flexible Electronics (Future Technologies), Nanjing Tech University, Nanjing 211816, China
*   Correspondence: chenghao@njtech.edu.cn (H.C.); pengnb@hyit.edu.cn (N.P.)

Abstract: With rapid economic development and a continuous increase in motor vehicle numbers, traffic congestion on highways has become increasingly severe, significantly impacting traffic efficiency and public safety. This paper proposes and investigates a traffic congestion prediction and emergency lane development strategy based on object detection algorithms. Firstly, the YOLOv11 object detection algorithm combined with the ByteTrack multi-object tracking algorithm is employed to extract traffic flow parameters—including traffic volume, speed, and density—from videos at four monitoring points on the Changshen Expressway in Nanjing City, Jiangsu Province, China. Subsequently, using an AdaBoost regression model, the traffic density of downstream road sections is predicted based on the density features of upstream sections. The model achieves a coefficient of determination R^2 of 0.968, a mean absolute error of 11.2 vehicles/km, and a root mean square error of 19.9 vehicles/km, indicating high prediction accuracy. Building on the interval occupancy rate model, this paper further analyzes the causes of traffic congestion and designs decision-making processes for the activation and deactivation of emergency lanes. By real-time monitoring and calculating the vehicle occupancy rate of the CD interval, threshold conditions for activating emergency lanes are determined. When the interval occupancy rate $K_{CD}(t)$ exceeds 80%, the emergency lane is proactively opened. This method effectively alleviates traffic congestion and reduces congestion duration. Quantitative analysis shows that after activating the emergency lane, the congestion duration in the CD section decreases from 58 min to 30 min, the peak occupancy rate drops from 1 to 0.917, and the congestion duration is shortened by 48.3%. Additionally, for the Changshen Expressway, this paper proposes two optimization points for monitoring point layout, including setting up monitoring points in downstream sections and in the middle of the CD section, to further enhance the scientific and rational management of emergency lanes. The proposed strategy not only improves the real-time extraction and prediction accuracy of traffic flow parameters but also achieves dynamic management of emergency lanes through the interval occupancy rate model, thereby alleviating highway traffic congestion. This has significant practical application value.

Keywords: traffic management; emergency lane; object detection (YOLOv11); ByteTrack; interval occupancy rate; congestion prediction

1. Introduction

With rapid economic development, the traffic load on highway systems is increasing daily, leading to increasingly severe traffic congestion problems, especially during holidays. Frequent traffic congestion not only affects people's quality of life but also causes significant economic losses. According to reports, in 2011, the global economic loss due to

travel delays and fuel consumption reached as high as USD 121 billion [1]. In China, the estimated economic loss caused by traffic congestion in the top 15 cities each day amounts to CNY 1 billion [2]. Additionally, traffic congestion exacerbates air pollution and fuel consumption [3], further impacting residents' quality of life and production efficiency [4]. Simultaneously, traffic congestion severely hinders the timely response capabilities of emergency vehicles such as ambulances and fire trucks.

During highway construction, emergency lanes are usually added on the right side to cope with engineering rescue, firefighting, medical aid, and other emergencies. As lifesaving channels, emergency lanes are closed to arbitrary occupation. However, if they can be used under reasonable circumstances—such as by monitoring the upstream and downstream traffic flow of a certain road section, predicting potential congestion, and opening the emergency lane in the absence of accidents to timely reduce traffic density—it is expected that large-scale congestion can be avoided [5]. Studies have shown that opening emergency lanes can significantly enhance highway traffic capacity and reduce response times in emergencies. By rationally utilizing emergency lanes, vehicles can bypass traffic congestion and quickly pass through accident or fault sections, thereby reducing traffic delays [6,7]. In this context, alleviating traffic pressure and effectively utilizing existing road resources have become primary tasks for traffic management departments, and the flexible use of emergency lanes is regarded as a potential solution [8,9].

Traffic congestion prediction and mitigation methods can be categorized into model-based and data-driven approaches [10]. Model-based methods predict future traffic parameters (e.g., occupancy, flow, or speed) by constructing traffic models, such as the Cell Transmission Model [11], queuing theory [12], and macroscopic traffic flow models [13]. These methods provide straightforward interpretations due to their clear physical foundations (e.g., flow dynamics). However, their idealized modeling assumptions struggle to accommodate the increasing traffic volume and complexity of modern transportation networks, leading to limitations in predictive accuracy for practical applications. Data-driven methods predict travel times and congestion by extracting features from traffic data. Traditional data-driven approaches include linear regression [14,15], autoregressive models [16], Kalman filtering [17,18], and Bayesian inference [19], which make predictions based on assumed probability distributions of the data. In recent years, machine learning methods such as k-Nearest Neighbors (kNN), Support Vector Machines (SVM), Artificial Neural Networks (ANN), and Random Forests (RF) have been widely applied in traffic flow prediction [20,21]. Deep learning models, in particular, have achieved significant progress through specific framework designs and improvements, as summarized in Table 1.

Table 1. Recent Deep Learning Frameworks for Traffic Congestion Prediction.

References	Time	Method	Results
Jiang et al. [22]	2024	AMCNN-ED (Attention-based multi-context convolutional encoder-decoder neural network)	Evaluated using four-year Maryland traffic data, achieving 5–34% reduction in speed prediction error, 11–29% in queue length, 6–17% in congestion timing, and 5–7% improvement in incident prediction accuracy compared to baselines.
Wang et al. [23]	2024	Hybrid model combining ARIMA, CNN-LSTM, and XGBoost	Demonstrated superior predictive accuracy with R^2 reaching 0.9874, significantly outperforming benchmark models.
Zechin et al. [24]	2023	Variational LSTM	Effectively controlled traffic anomalies while handling multiple independent variables and integrating with traffic management strategies.
Zhang et al. [25]	2024	Hybrid architecture combining Graph Neural Networks and Temporal Convolutional Networks	Achieved enhanced prediction accuracy compared to existing baselines, effectively forecasting different congestion levels (mild, moderate, severe) with computational efficiency suitable for large-scale road networks.

Table 1. *Cont.*

References	Time	Method	Results
Gao et al. [26]	2022	Improved CEEMDAN-FE-TCN model	Enhanced CEEMDAN algorithm successfully decomposed traffic flow time series of different frequencies, achieving significantly higher prediction accuracy after reconstruction.
Li et al. [27]	2024	Spatio-Temporal Graph Convolution Network with embedded location and time features (STEGCN)	Demonstrated superior performance in handling large-scale, structurally complex data compared to traditional methods (VAR, ARIMA, SVR), achieving RMSE = 23.71 on the PEMS08 dataset.

However, deep learning models face significant challenges due to their black-box nature and the complexity of traffic flow data (i.e., spatiotemporal dependencies) [28]. Ei Leen et al. [29] reviewed machine learning applications in mitigating traffic congestion for smart and sustainable cities, highlighting deficiencies in data reliability and model interpretability. Modi et al. [30] comprehensively reviewed intelligent traffic management using machine learning algorithms, noting that varying weather conditions and population densities make intelligent traffic management systems a challenging research task requiring further improvements in traffic flow and congestion prediction.

Current GCNN and DCNN-based models, despite their excellent performance on specific datasets, exhibit poor generalization capabilities, primarily because they treat spatial dependencies as static values without considering dynamic changes in input and traffic conditions. Hayeri et al. [31], after analyzing over 100 articles, found that 74% of studies focus on prediction alone, lacking targeted emergency lane activation strategies. Furthermore, traditional traffic flow parameter collection methods (e.g., induction loops, microwave radars, and video detectors) suffer from high installation and maintenance costs, limited coverage, and environmental sensitivity [32,33].

To address these challenges, this paper proposes an emergency lane activation strategy based on the YOLOv11 object detection algorithm. The strategy offers three key innovations:

1. Utilizes existing surveillance camera infrastructure for traffic flow parameter extraction without additional hardware investment;

2. Employs deep learning object detection algorithms for traffic flow parameter extraction, enhancing model intuition and interpretability;

3. Designs emergency lane activation and deactivation strategies based on interval occupancy rates, incorporating clear physical significance for improved applicability and reliability.

2. Data

The video data used in this study come from four traffic monitoring points on the Changshen Expressway in Nanjing City, Jiangsu Province, China. The specific locations are shown in Figure 1. From upstream to downstream, the four monitoring points are named A, B, C, and D, respectively. The duration statistics of the surveillance videos obtained from these four intersections are summarized in Table 2. Considering that traffic congestion frequently occurs in the CD section, designing a reasonable emergency lane activation strategy for this section has significant practical importance.
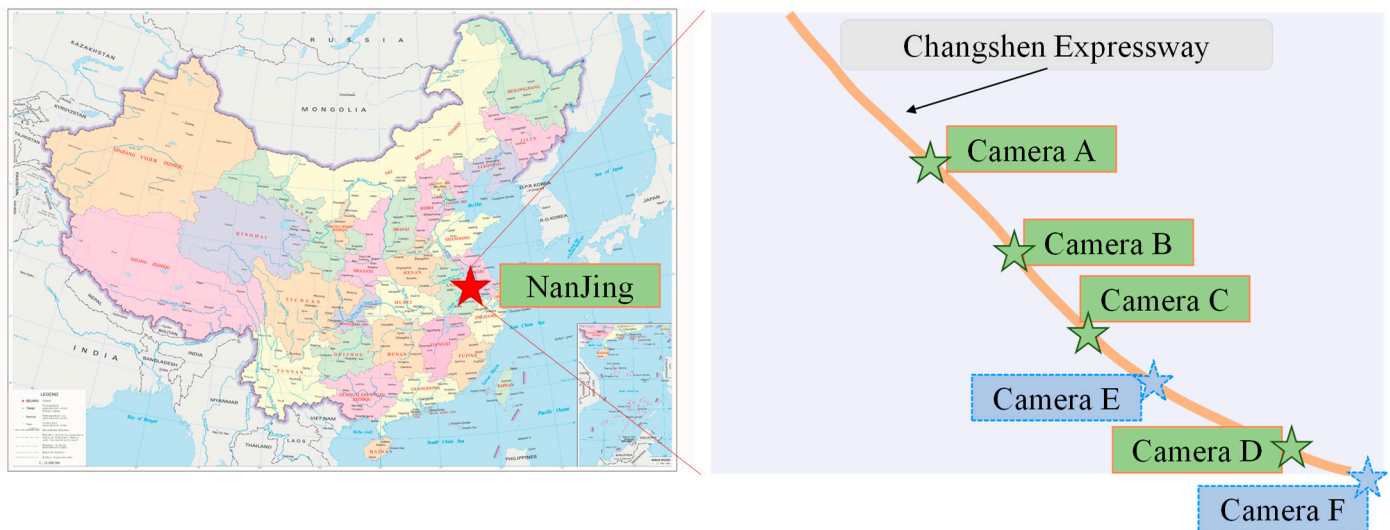
Figure 1. Locations of the four video monitoring points (Cameras E and F do not currently exist; they are proposed monitoring points to be added later in this paper to optimize the emergency lane activation strategy).

Table 2. Statistics of video information at the four observation points.

Observation Point	Start Time	End Time	Total Duration
A	2024-05-01 11:41:03	2024-05-01 16:14:32	4 h 33 min 29 s
B	2024-05-01 11:52:27	2024-05-01 15:28:20	3 h 35 min 53 s
C	2024-05-01 11:35:43	2024-05-01 16:09:12	4 h 33 min 29 s
D	2024-05-01 12:56:47	2024-05-01 15:20:04	2 h 23 min 17 s

3. Methodology

This paper combines video data from highway intersections to establish a traffic congestion prediction and emergency lane decision-making framework based on object detection algorithms. As shown in Figure 2, the system framework is a four-layer architecture consisting of the perception layer, data processing layer, software layer, and application layer. The perception layer collects traffic data using various cameras; there are already four cameras (A–D) on the Changshen Expressway, and cameras E and F are proposed in this paper to further enhance the rationality of the decision-making framework. The data processing layer uses YOLOv11, ByteTrack, and the Line-crossing Statistics method designed in this paper to obtain traffic flow data (q, u, ρ). The software layer includes real-time traffic monitoring, data visualization, historical data analysis, and congestion prediction modules. Finally, the application layer implements functions such as traffic monitoring processing, interval occupancy rate monitoring, and emergency lane deployment.
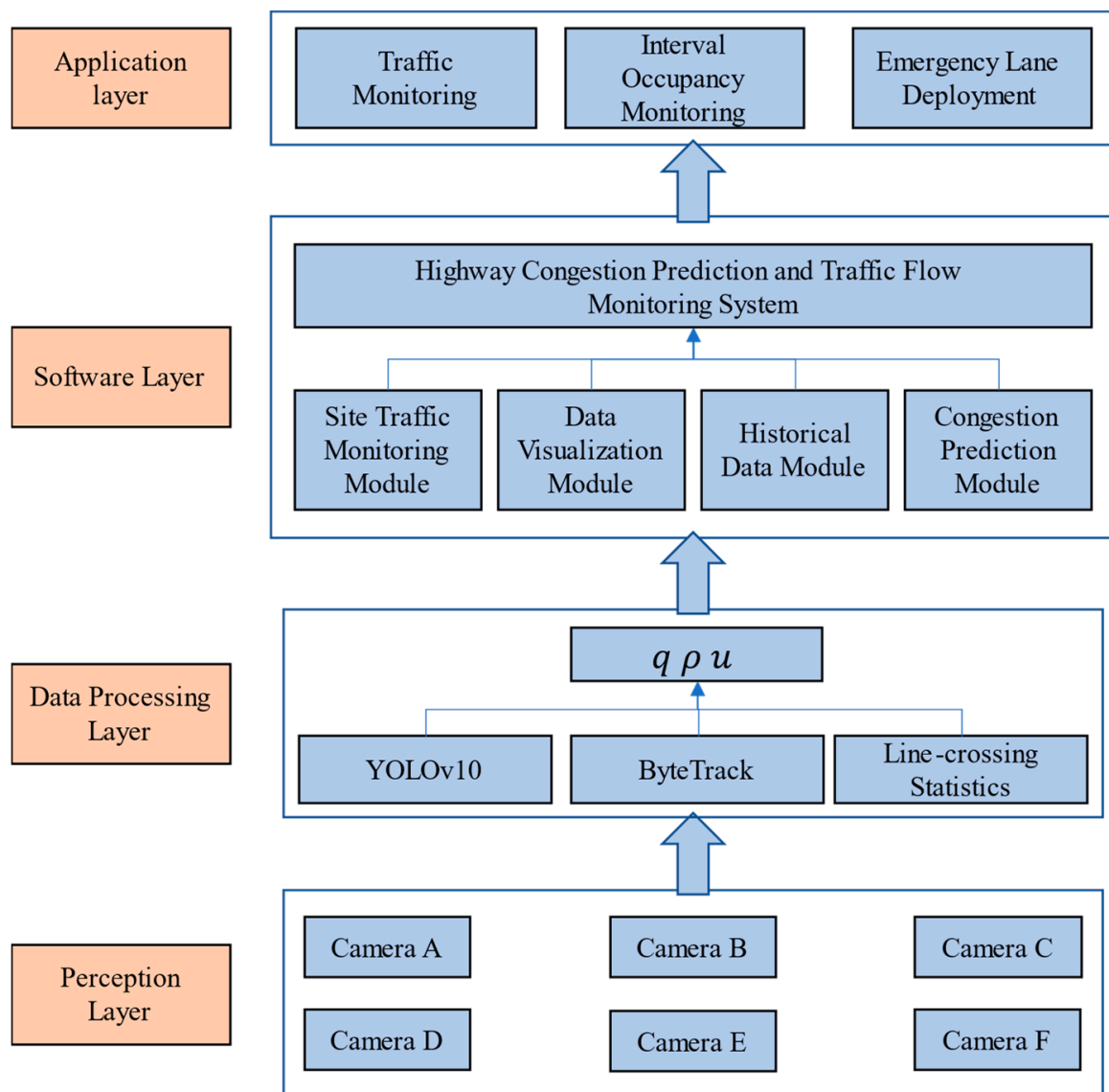
Figure 2. System framework design.

3.1. YOLOv11

Deep learning-based object detection methods mainly include two categories: two-stage detection algorithms (e.g., R-CNN [34], Fast R-CNN [35], Faster R-CNN [36,37]) and one-stage detection algorithms. While two-stage algorithms offer high accuracy, their complex processes limit real-time applications. In contrast, one-stage algorithms like YOLO series [38] and SSD [39] achieve efficient real-time detection and have gained widespread practical applications [40].

The YOLO series has evolved continuously to its latest version, YOLOv11 [41], released by Ultralytics in 2024. YOLOv11 adopts a Feature Pyramid Network (FPN) [42] structure with three main components: backbone network for feature extraction, neck for multi-scale feature fusion, and detection head for object detection and classification [43], as shown in Figure 3. Compared to previous versions, YOLOv11 introduces an efficient feature fusion mechanism and optimized lightweight design, enabling faster detection while maintaining high accuracy.
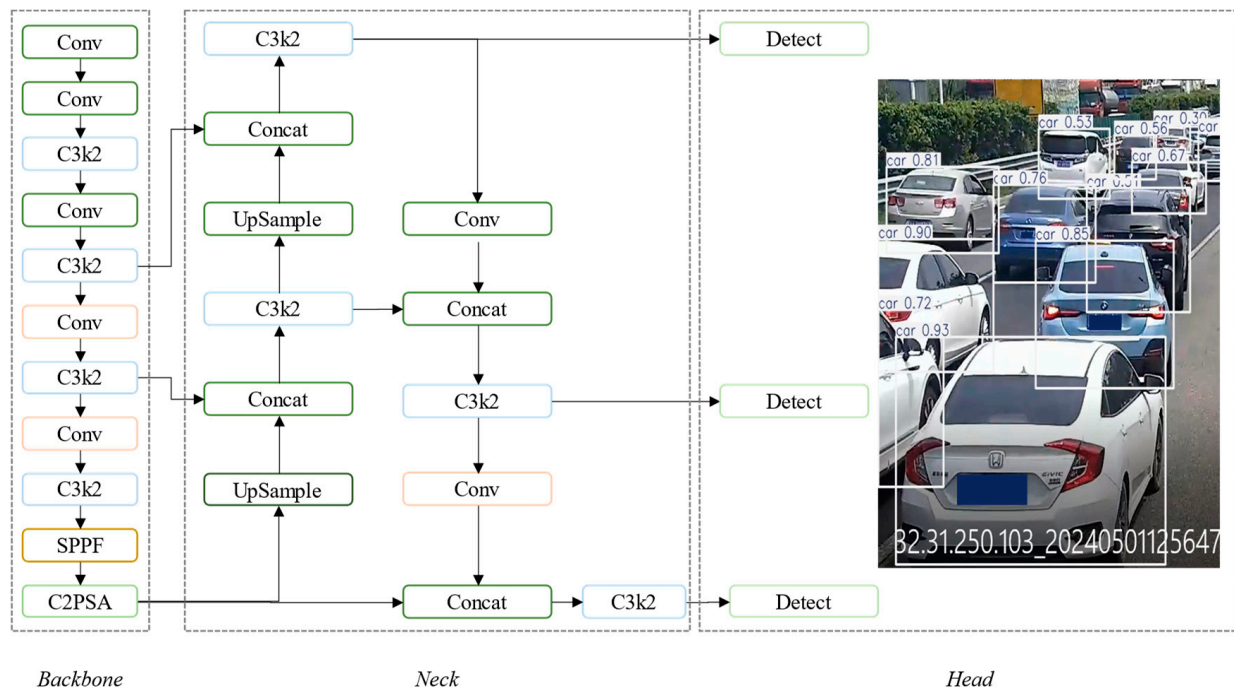
Figure 3. YOLOv11 model architecture.

In this study, we employ YOLOv11m, which achieves an optimal balance between detection accuracy and computational efficiency. With 22% fewer parameters compared to YOLOv8m while maintaining high precision, YOLOv11m provides efficient and accurate vehicle detection capabilities for real-time traffic flow parameter extraction and congestion prediction.

3.2. ByteTrack

ByteTrack [44] is a multi-object tracking algorithm based on object detection, aiming to achieve precise object tracking by associating all detection boxes—including both high-confidence and low-confidence detection boxes. Unlike traditional multi-object tracking algorithms that only use high-confidence detection boxes, ByteTrack fully considers low-confidence detection results, significantly improving tracking performance in complex scenes such as object occlusion and rapid movement.

In the ByteTrack algorithm, an object detector (such as the YOLOv11m used in this paper) is first used to perform object detection on each frame, obtaining a series of detection boxes and their corresponding confidence scores. Then, based on a preset confidence threshold, the detection boxes are divided into high-confidence and low-confidence categories. For high-confidence detection boxes, the Hungarian algorithm [45] is used to perform data association based on the Intersection over Union (IoU) between the detection boxes and existing trajectories, achieving reliable tracking of high-confidence objects. Specifically, the IoU distance between high-confidence detection boxes in the current frame and the predicted positions of trajectories in the previous frame is calculated to construct a cost matrix, and the Hungarian algorithm is used to solve the optimal matching.

For unmatched low-confidence detection boxes, ByteTrack includes them in the association process and performs matching again to supplement and refine object trajectories. This effectively solves tracking interruption problems caused by object occlusion or fluctuations in detector confidence.

Steps of the ByteTrack algorithm can be summarized as follows:

1. Object Detection: Perform object detection on the input frame to obtain all detection boxes and their confidences.

2. Classification: Divide detection boxes into high-confidence and low-confidence categories based on the confidence threshold.
3. First Matching: Use the Hungarian algorithm to perform the first matching between high-confidence detection boxes and existing trajectories.
4. Second Matching: For unmatched trajectories and low-confidence detection boxes, perform matching again to further refine trajectory information.
5. Update Trajectories: Update trajectory states and output tracking results.

By fully utilizing all available detection information, ByteTrack can achieve significant performance improvements in multi-object tracking tasks, making it particularly suitable for vehicle tracking in real-time traffic monitoring. The algorithm is simple and efficient, easy to implement, and can maintain high tracking accuracy in complex traffic environments.

3.3. Vehicle Line-Crossing Statistics

In video analysis, by predefining a counting line, when a vehicle's movement trajectory intersects with this line, it is considered that the vehicle has passed that position, thereby achieving vehicle line-crossing statistics.

As shown in Figure 4, the horizontal straight line is the counting line, and the curve represents the vehicle's movement trajectory. Let the endpoints of the counting line be $P_1(x_1, y_1)$ and $P_2(x_2, y_2)$, and the endpoints of the trajectory segment formed by the vehicle's positions in two adjacent frames be $Q_1(x_3, y_3)$ and $Q_2(x_4, y_4)$. By calculating the direction vectors of the two line segments and their cross products, it can be determined whether the line segments intersect.
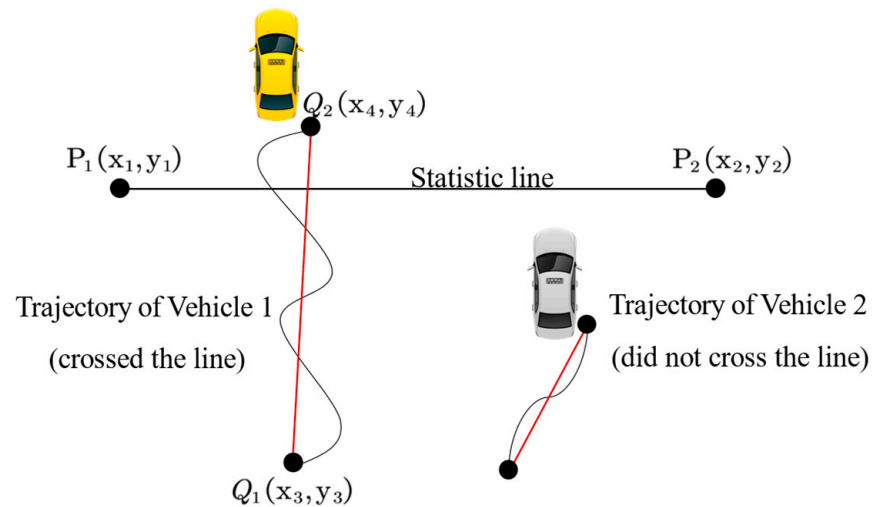
Figure 4. Illustration of line segment intersection determination.

The direction vector of the counting line segment is

$$\mathbf{D}_1 = P_2 - P_1 = (x_2 - x_1,\ y_2 - y_1) \tag{1}$$

The direction vector of the vehicle trajectory line segment is

$$\mathbf{D}_2 = Q_2 - Q_1 = (x_4 - x_3,\ y_4 - y_3) \tag{2}$$

Calculate the vector cross product $d = \mathbf{D}_1 \times \mathbf{D}_2$. If $d = 0$, the two vectors are parallel or colinear, and the line segments do not intersect, meaning the vehicle did not pass the counting line. If $d \neq 0$, further calculate the parameters t and u:

$$t = \frac{(Q_1 - P_1) \times \mathbf{D}_2}{d} \tag{3}$$

$$u = \frac{(Q_1 - P_1) \times \mathbf{D}_1}{d} \tag{4}$$

If $0 \le t \le 1$ and $0 \le u \le 1$, it indicates that the two line segments intersect, and the vehicle is determined to have passed the counting line.

Calculation of Basic Parameters

By combining YOLOv11 with ByteTrack and vehicle line-crossing statistics, we can obtain the total number of vehicles crossing the line, the average speed of the current vehicles, and the number of vehicles currently in the video. Based on these data, we can further calculate the three basic parameters of traffic flow: flow rate q, density ρ, and speed u.

Flow rate $q(x, t)$: The number of vehicles passing through position x within time t, measured in vehicles per hour (vehicles/h).

Density $\rho(x, t)$: The number of vehicles per unit length at position x at time t, measured in vehicles per kilometer (vehicles/km).

Speed $u(x, t)$: The average speed of vehicles passing through position x at time t, measured in kilometers per hour (km/h).

The calculation methods for each parameter are as follows:

1. Flow Rate $q(x, t)$

Flow rate represents the number of vehicles passing a certain position per unit time. Let N_n be the cumulative total number of vehicles crossing the line by the end of the n-th minute, then the flow rate in the n-th minute is

$$q_n = \frac{N_n - N_{n-1}}{\Delta t} \tag{5}$$

where Δt is the statistical time interval, in minutes. Similarly, the flow rate $q(x, t)$ for each time period can be calculated.

2. Density $\rho(x, t)$

Density represents the number of vehicles per unit length. Let N_n be the average number of vehicles in the n-th minute, and L be the effective length of the road within the camera's field of view. Then, the density in the n-th minute is

$$\rho_n = \frac{N_n}{L} \tag{6}$$

Similarly, the density $\rho(x, t)$ for each time period can be calculated.

3. Speed $u(x, t)$

Speed represents the average driving speed of vehicles passing through a certain position. Let v_n be the average vehicle speed in the n-th minute (unit: pixels/s). A unit conversion is needed to obtain km/h. Assuming the unit conversion factor is k, then the speed in the n-th minute is

$$u_n = v_n \times k \tag{7}$$

Similarly, the speed $u(x, t)$ for each time period can be calculated.

3.4. AdaBoost Regression

The AdaBoost regression algorithm is a classic ensemble learning algorithm based on an adaptive boosting strategy proposed by Freund and Schapire in 1996. The algorithm forms a stronger regression model by combining multiple weak regressors [46]. Through this combination, the overall predictive ability of the model can be significantly improved. The schematic diagram of the algorithm is shown in Figure 5.
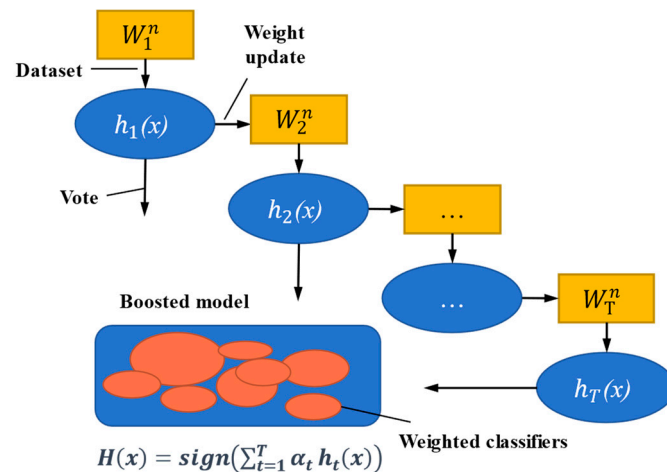
Figure 5. Schematic diagram of the AdaBoost algorithm.

In the adaptive iterative process, multiple weak regressors are interrelated, and the prediction error of each weak regressor will affect the weight distribution of samples in the next iteration [47]. Through this weight update mechanism, AdaBoost guides the model to focus more on samples that are difficult to predict in subsequent iterations, thereby improving the predictive performance of the overall model. Specific steps are as follows:

1. Initialization: In the initial stage of the algorithm, all training samples are assigned equal weights. At this time, each sample has the same importance for model training.

$$D_1(i) = (w_1, w_2, \ldots, w_N) = \frac{1}{N} \tag{8}$$

2. Iteration: Execute the iterative process, setting the number of iterations as $t = 1, \ldots, T$, where $\mathcal{X}$ represents the input space, y_i represents the actual target value, and $h_t(x_i)$ is the predicted value from the weak regressor.

3. Compute Error: Calculate the error ϵ_t of the weak regressor $h_t(\mathcal{X})$ under the weight distribution D_t, which measures the predictive effect of the current weak regressor on the overall samples.

$$\epsilon_t = \frac{\sum_{i=1}^{N} w_n(t) \cdot |h_t(x_i) - y_i|}{\sum_{i=1}^{N} w_n(t)} \tag{9}$$

The error ϵ_t is the weighted absolute error, reflecting the performance of the current weak regressor.

4. Compute Regressor Weight: Calculate the weight α_t of the weak regressor in the final model based on the size of the error. The weight reflects its importance in the combined model; the smaller the error, the higher the weight.

$$\alpha_t = \log\left(\frac{1 - \epsilon_t}{\epsilon_t}\right) \tag{10}$$

5. Update Sample Weights: Update the weight distribution D_{t+1} of each sample. Samples with larger errors will receive higher weights, while samples with better prediction effects will reduce their weights.

$$D_{t+1}(i) = D_t(i) \cdot \exp(|h_t(x_i) - y_i|) \tag{11}$$

This process ensures that in subsequent iterations, the model will increasingly focus on samples with larger prediction errors, continuously optimizing the predictive effect of the model.

6. Final Model Formation: After *T* iterations, AdaBoost forms the final strong regression model by combining all the weak regressors and weighting them according to their weights α_t:

$$H(x) = \sum_{t=1}^{T} \alpha_t \cdot h_t(x) \tag{12}$$

3.5. Interval Occupancy Rate Model

As shown in Figure 6, taking the BC interval as an example, suppose the vehicle flow rates at point B and point C at time *t* are $q_B(t)$ and $q_C(t)$, respectively. When $q_C(t)$ continues to be less than $q_B(t)$, it indicates that fewer vehicles are exiting than entering, leading to an increasing number of vehicles within the BC interval. These accumulated vehicles will reach the downstream CD section after some time. Therefore, when the vehicle occupancy rate within the BC interval reaches 80% of its maximum capacity Q_m, the emergency lane of the CD section should be activated in advance.
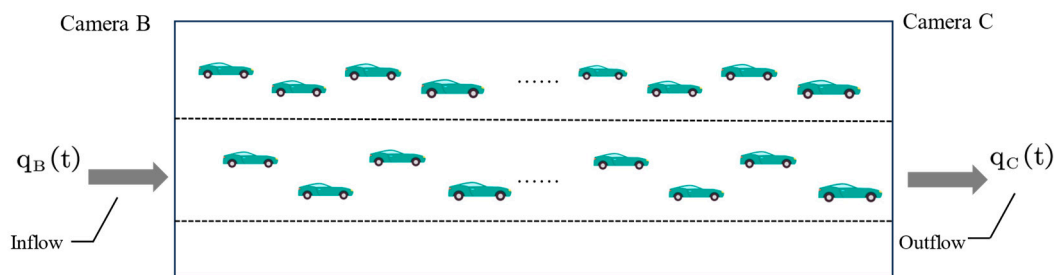

Figure 6. Schematic diagram of vehicle occupancy in an interval; When the number of entering vehicles continues to exceed the number of exiting vehicles, traffic congestion forms.

Benefits of activating the emergency lane in advance:

1. Alleviate Upstream Congestion: Since the CD section is downstream, after opening the emergency lane, its traffic capacity is enhanced, increasing the flow rate $q_C(t)$ at point C, thereby alleviating the traffic pressure in the BC interval.

2. Provide Buffer Space: The activation of the emergency lane can accelerate the clearing of vehicles within the CD section, providing a larger buffer space for incoming vehicles and reducing congestion risk.

3. Increase Traffic Capacity: Opening the emergency lane directly increases the traffic capacity of the CD section, preparing for the large inflow of vehicles and preventing the occurrence of traffic congestion.

Let Q_m (unit: vehicles) be the maximum vehicle capacity of the BC interval, and Q_0 be the number of vehicles in the interval at the initial moment ($t = 0$). Then, the total number of vehicles $Q(t)$ within the BC interval at time *t* is

$$Q(t) = Q_0 + \int_0^t [q_B(\tau) - q_C(\tau)]d\tau \tag{13}$$

where τ is the integration variable, and $q_B(\tau) - q_C(\tau)$ represents the net inflow at time τ. To determine whether it is necessary to open or close the emergency lane, define the vehicle occupancy rate $K_{BC}(t)$ of the BC interval as

$$K_{BC}(t) = \frac{Q(t)}{Q_m} = \frac{Q_0 + \int_0^t [q_B(\tau) - q_C(\tau)]d\tau}{Q_m} \tag{14}$$

When $K_{BC}(t)$ exceeds 80%, it indicates that the number of vehicles in the BC interval has reached 80% of its maximum capacity. At this time, congestion may form, and the emergency lane of the downstream CD section should be activated in advance:

$$\text{If } K_{BC}(t) > 0.8, \text{then open the emergency lane} \tag{15}$$

Conversely, when $K_{BC}(t)$ drops below 60%, it indicates that the number of vehicles in the interval has significantly decreased, and the emergency lane can be closed to ensure its normal function for emergency passage:

$$\text{If } K_{BC}(t) < 0.6, \text{then close the emergency lane} \tag{16}$$

Therefore, by calculating the vehicle occupancy rate $K_{BC}(t)$ in real time, the traffic conditions of the BC interval can be effectively monitored, and strategies for opening or closing the emergency lane can be timely implemented, enhancing road traffic efficiency and safety.

4. Results

4.1. Traffic Flow Data Extraction Results and Analysis

As illustrated in Figure 7, the process of extracting traffic flow data using YOLOv11 combined with the ByteTrack algorithm and the line-crossing statistics method is shown. The black lines correspond to vehicle trajectories, and the ID numbers are assigned to each vehicle by the object tracking algorithm. "Conf" represents the confidence level of the detection results from the object detection algorithm, and a higher confidence level indicates a higher probability that the detected object is a vehicle.
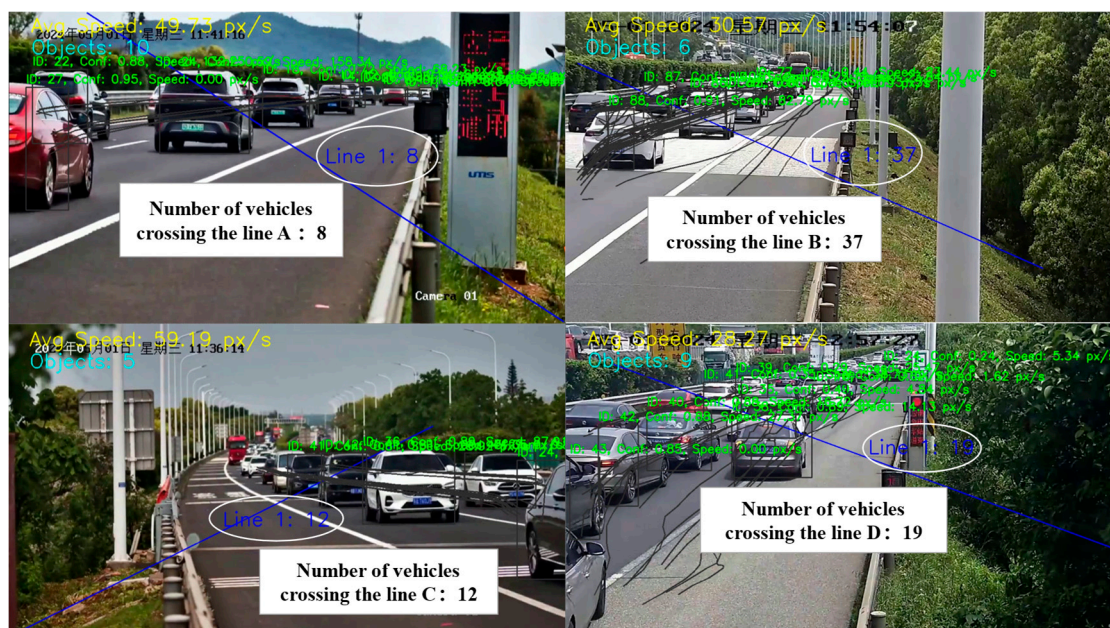

Figure 7. Object detection and information extraction process.

The obtained flow rate, density, and speed data are plotted as time–history curves, as shown in Figure 8. It can be observed that the flow rate and density curves exhibit very similar trends, showing higher values in the earlier period and lower values later. This indicates that at the beginning of the observation, vehicle traffic was relatively dense, and as time progressed, the traffic volume gradually decreased. After smoothing the density curves (as shown in Figure 9), the consistency of the trends and propagation characteristics of the traffic flow parameters are more clearly demonstrated. The density curves of the four

observation points all display similar "Z"-shaped characteristics, that is, they are higher initially and lower later along the time axis. This trend has a certain transmission over time, manifesting as sequential propagation from the upstream intersections A, B, and C to the downstream intersection D.
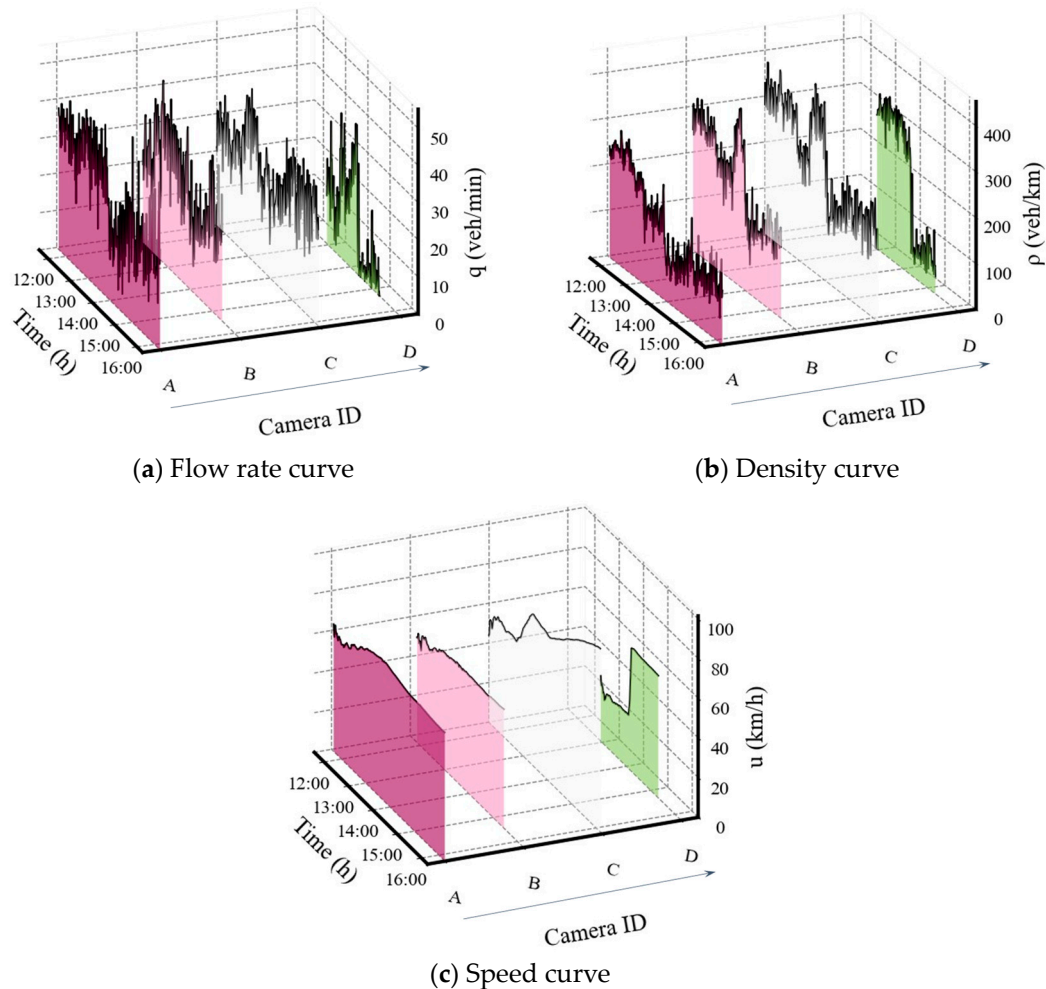

(**a**) Flow rate curve

(**b**) Density curve

(**c**) Speed curve

Figure 8. Time–history curves of traffic flow parameters.
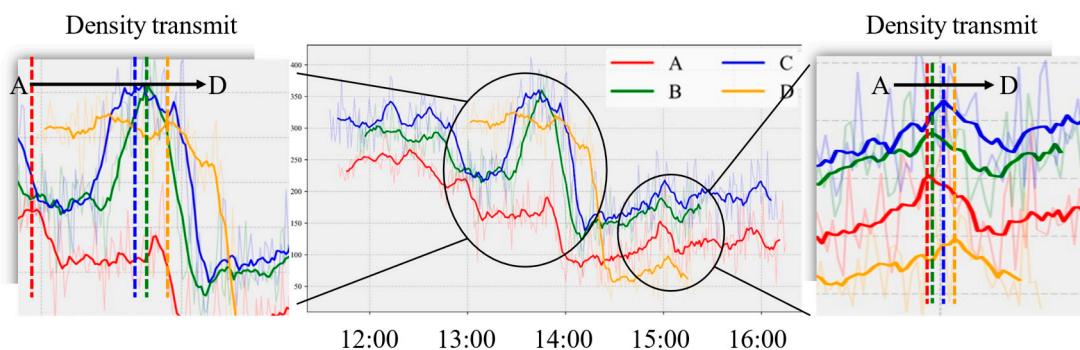

Figure 9. Smoothed density curves.

Specifically, due to the distances between the intersections, vehicles require a certain travel time from upstream to downstream, resulting in a time lag effect in the traffic flow parameters. The distances between observation points A, B, and C are relatively close (approximately 1 km), so the time lag Δt is small. The distance between observation point

D and point C is greater (3 km), so the time lag is more significant, with Δt being relatively large. Additionally, due to traffic congestion occurring at intersection D, the flow rate and speed curves at this point show significant differences from those at upstream intersections A, B, and C, especially in the speed curve. This difference reflects the impact of traffic congestion on downstream traffic flow and validates the effectiveness of the traffic flow parameter extraction method based on video data proposed in this paper.

4.2. Traffic Flow Density Prediction

Based on the previous analysis, it is evident that the upstream traffic flow on the highway will reach the downstream section after a certain time delay, indicating a correlation between the traffic flow densities of the upstream and downstream. Therefore, this section aims to utilize the density characteristics of the upstream observation points A, B, and C to predict the traffic flow density at the downstream observation point D using the AdaBoost regression model.

First, a correlation analysis of the density characteristics between observation points was conducted. As shown in Figure 10, the correlation heatmap of the density characteristics between the observation points is presented. The results indicate that the correlation coefficients between the densities at observation points A, B, and C over the previous 10 min and the density at observation point D are 0.73, 0.75, and 0.79, respectively—all exceeding 0.7. This demonstrates a strong positive correlation between the density characteristics of the upstream observation points and the density at the downstream observation point D. Moreover, considering the distance relationships between the observation points (i.e., AD > BD > CD), the magnitude of the correlation coefficients is inversely proportional to the distance—the closer the distance, the stronger the correlation. This result aligns with the actual conditions in traffic flow theory, where the influence of upstream traffic flow on downstream diminishes with increasing distance.
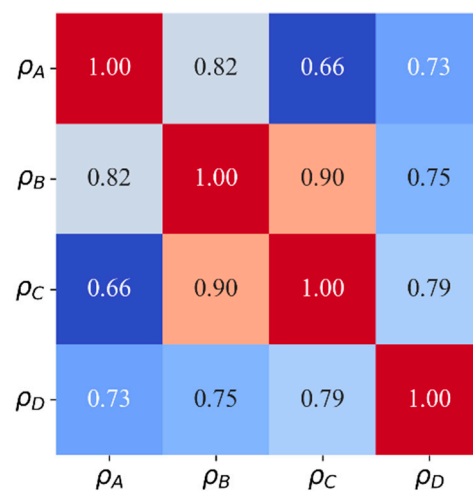

Figure 10. Density correlation between observation points.

In terms of data preparation, since the video data are not completely overlapped, the non-overlapped front and rear video data are not used. A total of 134 min of data were obtained from the video of observation point D, corresponding to 134 sample points. To build and evaluate the prediction model, the data were randomly divided into training and test sets in a 0.5:0.5 ratio. The input features of the model are the traffic flow densities at observation points A, B, and C at time t, and the target variable is the traffic flow density at observation point D at time $t + 10$ min.

The prediction results of the test set are shown in Figure 11. It can be observed that the density values predicted by the model closely match the actual observed values, reflecting the model's strong ability to capture changes in traffic flow density. Further performance evaluation metrics indicate that the model's coefficient of determination R^2

reaches 0.968, the mean absolute error (MAE) is 11.2 vehicles/km, and the root mean square error (RMSE) is 19.9 vehicles/km. These metrics demonstrate that the AdaBoost regression model possesses high accuracy and reliability in predicting traffic flow density.
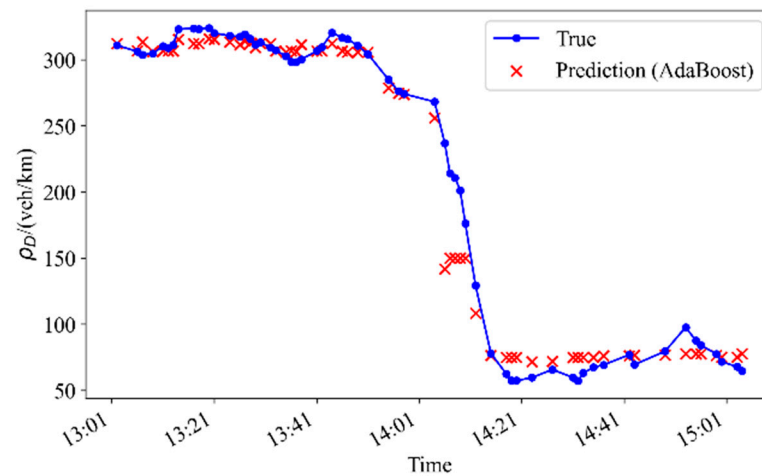

Figure 11. Actual density at observation point D and density predicted by the AdaBoost model.

To gain deeper insight into the model's prediction mechanism, an importance analysis of the input features was conducted. As shown in Figure 12, the relative importance of the density characteristics of observation points A, B, and C in the model prediction process is presented. The results reveal that observation point C has the highest importance, followed by observation point B, with observation point A having the lowest importance—that is, the feature importance satisfies C > B > A. This is inversely proportional to the distances between the observation points and the target observation point D—the closer the distance, the greater the contribution to the prediction. This result is consistent with the previous correlation analysis and conforms to the physical laws of traffic flow propagation, further validating the rationality of the model's decision-making process.
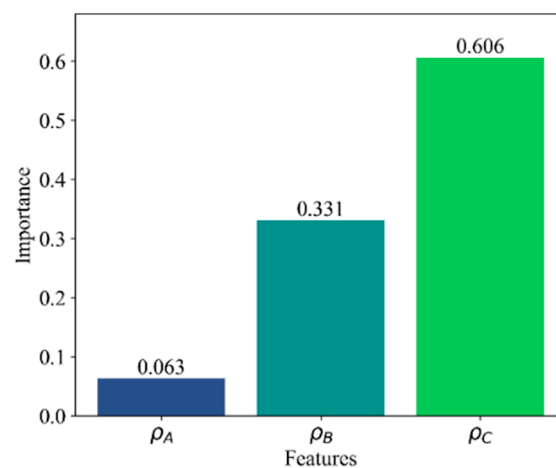

Figure 12. Importance of densities at intersections A, B, and C in predicting the density at intersection D.

Therefore, by fully utilizing the density characteristics of the upstream observation points, the AdaBoost regression model can effectively predict the traffic flow density at the downstream observation point. The model's high-precision predictions and reasonable distribution of feature importance provide solid data support and a theoretical basis for traffic congestion early warning and emergency lane activation strategies.

4.3. Analysis of Congestion Causes and Emergency Lane Activation Process

This section utilizes the interval occupancy rate model to analyze the causes of traffic congestion on the Changshen Expressway and, based on this, proposes an emergency lane activation process for the CD section grounded on the interval occupancy rate.

First, focusing on the CD interval, the changes in vehicle accumulation and occupancy rate are analyzed. According to the aforementioned theoretical model, the change in the number of vehicles within the interval can be expressed as

$$Q(t) = Q_0 + \int_0^t [q_C(\tau) - q_D(\tau)]d\tau \tag{17}$$

where $q_C(t)$ and $q_D(t)$ represent the traffic flow rates passing through points C and D at time t, respectively; Q_0 is the initial number of vehicles within the interval; $Q(t)$ is the total number of vehicles within the interval at time t. The interval occupancy rate $K_{CD}(t)$ is defined as

$$K_{CD}(t) = \frac{Q(t)}{Q_m} \tag{18}$$

where Q_m is the maximum vehicle capacity of the CD interval. Based on the collected traffic flow data, as shown in Table 3, a phased analysis of the congestion process in the CD interval was conducted.

Table 3. Traffic flow rates at intersections C and D.

Stage	Time	$q_C(t)$	$q_D(t)$	$q_C(t) - q_D(t)$
Early Stage	2024-05-01 13:04:00	37.7	23.01	14.69
	2024-05-01 13:05:00	37.2	23.27	13.93
	2024-05-01 13:06:00	36.3	22.49	13.81
	...	...	...	
Middle Stage	2024-05-01 14:09:00	21.6	37.96	−16.36
	2024-05-01 14:10:00	21.7	39.26	−17.56
	2024-05-01 14:11:00	21.8	40.69	−18.89
	2024-05-01 14:12:00	22.3	40.04	−17.74
	2024-05-01 14:13:00	22.2	38.35	−16.15
Later Stage	...	...	...	
	2024-05-01 15:10:00	29.4	6.63	22.77
	2024-05-01 15:11:00	27.9	5.59	22.31
	2024-05-01 15:12:00	27.9	5.33	22.57

The above process can be visually depicted in Figure 13. In the figure, the difference between the curves $q_C(t)$ and $q_D(t)$ reflects the net inflow of the CD interval. The blue areas represent the periods where $q_C(t) > q_D(t)$, indicating stages of increasing vehicle accumulation within the interval; the orange areas represent periods where $q_C(t) < q_D(t)$, indicating stages where vehicles in the interval are decreasing.
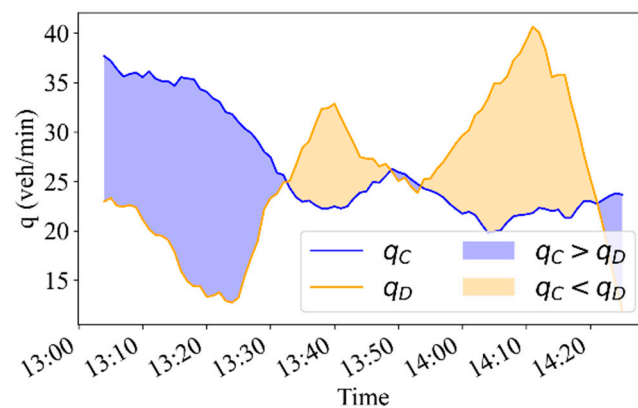

Figure 13. Traffic flow difference in the CD section.

Video monitoring at intersection D revealed that traffic congestion had formed by 13:04. As time progressed, the blue area continued to expand, indicating intensified vehicle accumulation within the interval and worsening congestion. Subsequently, due to the increase in $q_D(t)$ and decrease in $q_C(t)$, orange areas appeared—vehicles began to disperse, congestion gradually eased, and traffic conditions returned to normal.

Similarly, analyses were conducted for the AB and BC sections, and the corresponding traffic flow difference curves were plotted (Figures 14 and 15). The results show that the blue and orange areas in these sections alternate and are smaller in area, without forming severe traffic congestion like that in the CD section. This aligns with the actual video data, indicating that although brief traffic congestion occasionally occurs at intersections A, B, and C, the degree is mild and the duration short.
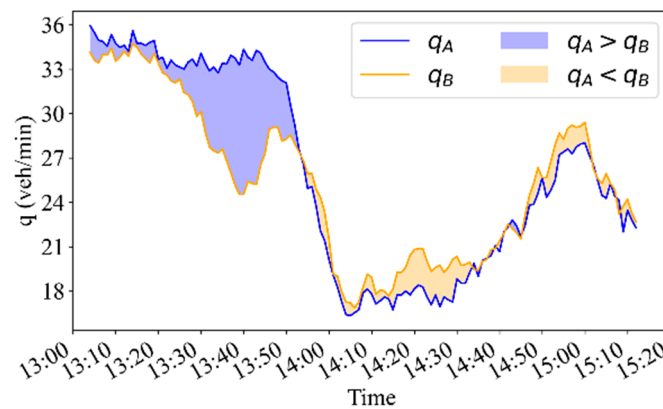

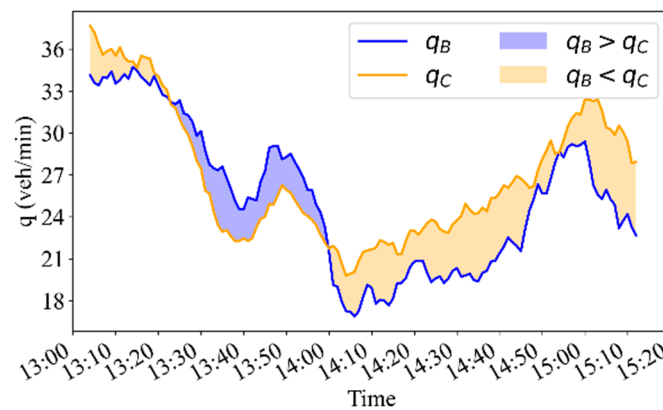**Figure 14.** Traffic flow difference in the AB section.

Figure 15. Traffic flow difference in the BC section.

The above analysis demonstrates that the interval occupancy rate model can effectively describe congestion situations between road sections, providing an important decision basis for whether to open the emergency lane. By integrating the existing monitoring camera layout of the Changshen Expressway, the emergency lane activation decision-making process shown in Figure 16 was designed.
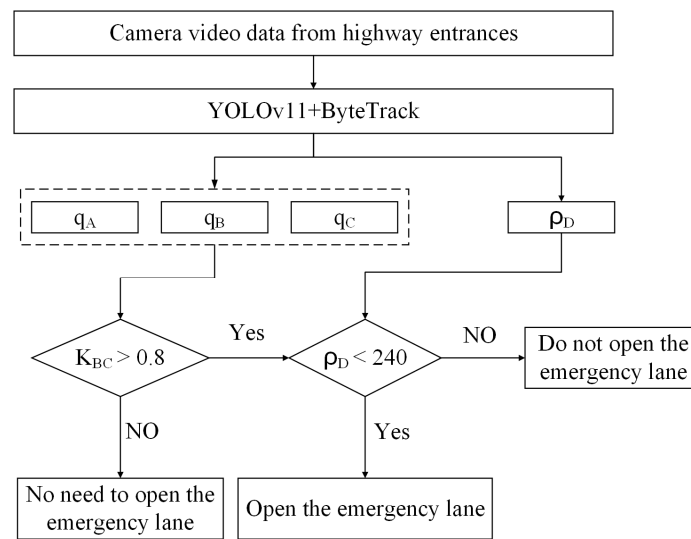
Figure 16. Emergency lane activation decision-making flowchart.

First, real-time video data are obtained from upstream observation points A, B, C, and downstream observation point D. The YOLOv11 and ByteTrack algorithms are utilized to extract traffic flow parameters at each intersection, including traffic flow rate $q(t)$ and density $\rho(t)$. Then, based on the collected data, the occupancy rate $K_{BC}(t)$ of the upstream BC interval is calculated according to Equation (19):

$$K_{BC}(t) = \frac{Q_0 + \int_0^t [q_B(\tau) - q_C(\tau)]d\tau}{Q_m} \tag{19}$$

where $q_B(t)$ and $q_C(t)$ are the traffic flow rates at points B and C, respectively; Q_m is the maximum vehicle capacity of the BC interval. When the occupancy rate $K_{BC}(t) > 0.8$ in the upstream BC interval (indicating that vehicle accumulation upstream may lead to downstream congestion) and the density at downstream intersection D satisfies $\rho_D(t) < 240$ vehicles/km (ensuring sufficient traffic capacity downstream), the emergency lane in the CD section is activated.

4.4. Quantitative Analysis of the Benefits of Emergency Lane Activation

This section employs the interval occupancy rate model to compare and analyze the traffic conditions of the CD section of the Changshen Expressway before and after the opening of the emergency lane, quantitatively evaluating the benefits resulting from the activation of the emergency lane.

First, determining the maximum capacity Q_m of the modeling interval is a crucial step in calculating the interval occupancy rate function $K(t)$. For the CD section (length $L_{CD} = 3$ km), two methods are used to estimate Q_m:

Method 1: Based on Maximum Traffic Density

Given that at 13:29, the traffic density of the CD section reaches the maximum value $\rho_{\max} = 325.9$ vehicles/km, according to $Q_m = \rho_{\max} \times L_{CD}$, we obtain: $Q_m = 977.7$ vehicles.

Method 2: Based on Occupancy Rate Change

Assuming that at 13:29, the interval occupancy rate reaches the maximum value $K(13:29) = 1$ (i.e., the interval is saturated), through video monitoring, it was found that by 14:10, the traffic congestion had eased. Assuming that the occupancy rate at this time drops to $K(14:10) = 0.8$, according to the relationship between occupancy rate change and net outflow:

$$\int_{13:29}^{14:10} [q_D(\tau) - q_C(\tau)]d\tau = [K(14:10) - K(13:29)]Q_m = (-0.2)Q_m \tag{20}$$

Given that $q_C(t)$ and $q_D(t)$ are observed data, the integral result calculated from the statistical data is

$$\int_{13:29}^{14:10} [q_D(\tau) - q_C(\tau)]d\tau = -238.6 \tag{21}$$

Therefore:

$$-238.6 = (-0.2)Q_m \Rightarrow Q_m = \frac{238.6}{0.2} = 1193 \tag{22}$$

Since Q_m represents the maximum capacity of the interval, the smaller of the estimated values should be taken to ensure a safety margin. Therefore, we take $Q_m = 977.7$ vehicles (rounded to 978 vehicles). Then, based on the estimated $Q_m = 978$ vehicles, the occupancy rate function $K(t)$ of the CD section when the emergency lane is not activated is calculated, obtaining

$$K(t) = K(t_0) + \frac{\int_{t_0}^{t} [q_C(\tau) - q_D(\tau)]d\tau}{Q_m} \tag{23}$$

where the initial moment $t_0 = 13:04$. Using Equation (24), we calculate $K(13:04) = 0.672$.

$$K(13:04) = 1 - \frac{\int_{13:04}^{13:29} [q_D(\tau) - q_C(\tau)]d\tau}{Q_m} \tag{24}$$

Substituting the actual observed $q_C(t)$ and $q_D(t)$ data into the above equations, the $K(t)$ curve is plotted (as shown in Figure 17). It can be observed that in the early stage, the value of $K(t)$ gradually increases, indicating vehicle accumulation within the interval and worsening congestion; when $K(t)$ reaches 1, the interval reaches saturation. Subsequently, $K(t)$ begins to decline, indicating that congestion is gradually easing.
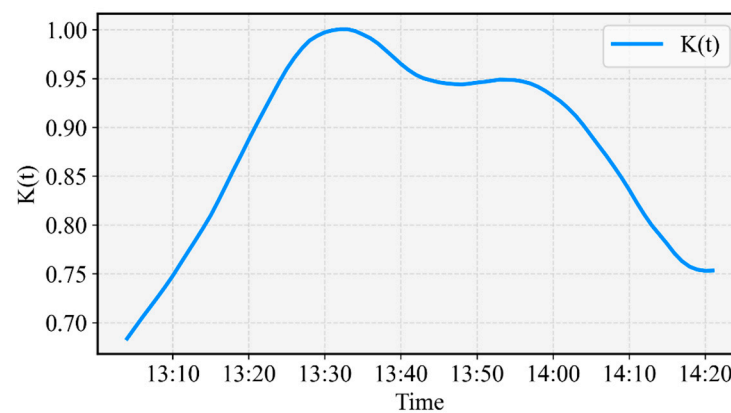

Figure 17. $K(t)$ curve when the emergency lane is not activated.

After activating the emergency lane, the CD section increases from two lanes to three lanes, enhancing traffic capacity. Assume that after activating the emergency lane, the traffic capacity of the CD section increases by 30%, i.e., the maximum passing capacity of vehicles increases by 30%. Since road capacity is directly related to the number of lanes, Q_m increases by 30%, so $Q_{m\prime} = Q_m \times 1.3 = 1271$. After enhancing traffic capacity, the number of vehicles passing through point D per unit time increases:

$$q_{D\prime}(t) = q_D(t) \times 1.3 \tag{25}$$

Considering the above changes, the occupancy rate function after activating the emergency lane is

$$K\prime(t) = K(t_0) + \frac{\int_{t_0}^{t} [q_C(\tau) - q_{D\prime}(\tau)]d\tau}{Q_{m\prime}} \tag{26}$$

That is:

$$K\prime(t) = 0.672 + \frac{\int_{13:04}^{t} [q_C(\tau) - 1.3q_D(\tau)]d\tau}{1271} \tag{27}$$

Comparing $K\prime(t)$ with $K(t)$ when the emergency lane is not activated (as shown in Figure 18), it can be found that after activating the emergency lane, the $K\prime(t)$ curve is overall lower than the $K(t)$ curve, indicating that vehicle accumulation within the interval decreases and the congestion situation improves.
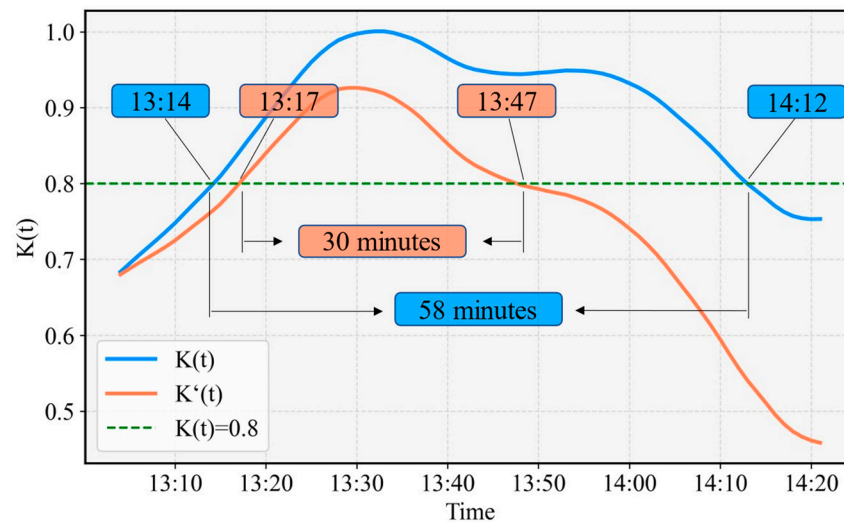

Figure 18. Comparison of $K(t)$ curves with and without activating the emergency lane.

Through the above analysis, the benefits brought by activating the emergency lane are quantitatively evaluated as follows:

1. Shortened Congestion Duration: Without activating the emergency lane, the congestion duration is 58 min (from 13:12 to 14:10), and after activating the emergency lane, the congestion duration is 30 min (from 13:15 to 13:45), reducing the congestion time by 28 min, a reduction of 48.3%.

2. Changes in Congestion Start and End Times: The congestion start time was delayed by 3 min (from 13:12 to 13:15), and the congestion end time was advanced by 25 min (from 14:10 to 13:45).

3. Reduced Peak Occupancy Rate: Without activating the emergency lane, $K_{max} = 1$, and after activating the emergency lane, $K\prime_{max} = 0.917$, reducing the peak occupancy rate by 8.3%.

These results indicate that after opening the emergency lane, the traffic capacity of the CD section is significantly improved, vehicle accumulation within the interval is effectively controlled, the degree of congestion is reduced, and the duration is shortened. This demonstrates that reasonable activation of the emergency lane plays an important role in alleviating traffic congestion and improving road traffic efficiency.

5. Discussion

The aforementioned emergency lane activation strategy is designed based on the existing camera arrangement. To enhance the scientific nature of the temporary activation decision for the emergency lane between the CD section while controlling costs, we can improve the rationality of emergency lane deployment by adjusting the positions of monitoring points or adding a small number of monitoring points.

5.1. Adding Point E at the Downstream Location

In the current scheme, only the single-point density at point D is considered, which cannot reflect the interval density of the downstream road section. If a camera at point E

is added downstream of point D, a vehicle occupancy rate model for the DE interval can be established. By calculating K_{DE}, we can determine whether congestion has occurred downstream, providing a basis for deciding whether to open the emergency lane in the CD section. The function of K_{DE} is similar to ρ_D, both aiming to ensure that there is no congestion ahead of the emergency lane. However, density ρ is an instantaneous variable with significant fluctuations, whereas K_{DE} can describe the overall congestion situation of the downstream DE interval, making it relatively more stable and reasonable. Therefore, after adding point E, the decision flowchart (Figure 16) can be improved, with the updated result shown in Figure 19.
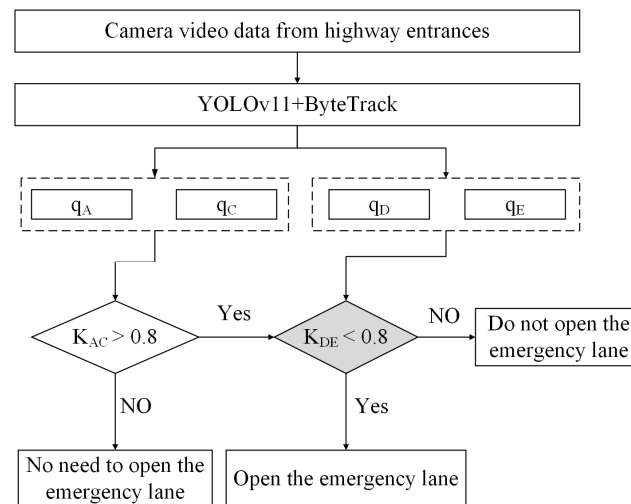

Figure 19. Emergency lane activation decision flowchart (after adding point E).

To avoid increasing costs, the camera at point B can be moved downstream of point D to serve as the new monitoring point E. The reason for removing the camera at point B instead of that at point A is that monitoring points A, B, and C are close to each other; segments AB and BC are both 1 km long, while the length of segment CD is 3 km. If the camera at point B is removed, the length of segment AC becomes 2 km; if the camera at point A is removed, segment BC remains 1 km. The longer AC interval results in its maximum capacity Q_{m-AC} being greater than Q_{m-BC}. According to the definition of occupancy rate, the longer the interval, the lower the sensitivity of $K(t)$ to traffic flow changes, and the more stable its response, which is beneficial for decision stability. In contrast, the occupancy rate $K_{BC}(t)$ of the shorter BC interval is more sensitive to short-term traffic flow changes, which may lead to overly frequent activation or deactivation of the emergency lane during the decision-making process. Therefore, by removing the camera at point B and using the longer AC interval to calculate the occupancy rate $K_{AC}(t)$, the reliability of the decision can be improved.

5.2. Adding Point F Within the CD Interval

The CD interval spans 3 km, which is relatively long. In the previous analysis, the vehicle occupancy rate within the interval was modeled based on statistical quantities from a few cameras, but it is challenging to obtain the utilization rate of each lane within the interval (especially the emergency lane). Therefore, to establish a lane utilization model, if costs permit, this paper proposes deploying a camera at point F within the CD section that can be used to detect the utilization rate of the emergency lane within the CD interval after activation, providing a basis for closing the emergency lane.

As shown in Figure 20, by using the YOLOv11 and ByteTrack algorithms combined with a vehicle decay factor, a heatmap can be generated for the areas where vehicles pass in the video data. The brighter areas in the heatmap indicate higher lane utilization. Based on this concept, the utilization rate of the emergency lane in the road section can be calculated,

providing a basis for closing the emergency lane after activation. If the utilization rate decreases to a certain level after a period, closing the emergency lane can be considered.
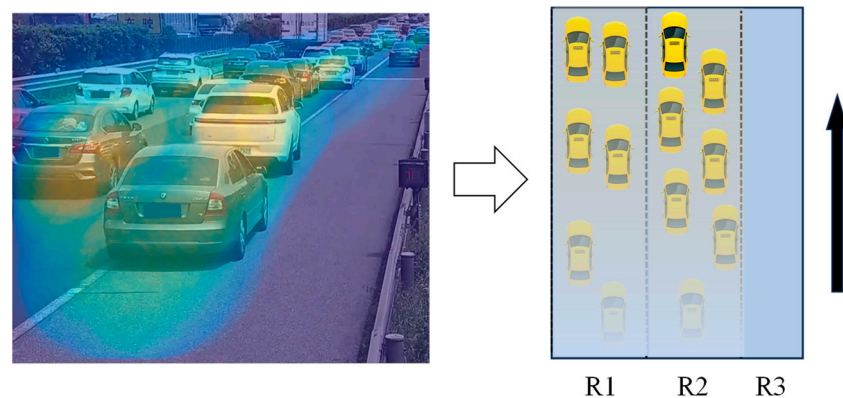

Figure 20. Lane division diagram.

In the heatmap, the value of each pixel reflects the frequency at which that position is occupied by vehicles over a period, essentially representing the spatial and temporal distribution density of vehicles. By using heatmap data, the utilization rate of each lane can be calculated, providing an important reference for deciding when to close the emergency lane.

1. Lane Area Division

As shown in Figure 20, the lanes are divided into three areas R_i ($i = 1, 2, 3$), where R_3 represents the emergency lane.

2. Calculating the Total Heat of Each Lane Area

The numerical results of the heatmap are calculated based on the vehicles detected in each frame combined with a decay factor, as shown in Equation (28):

$$\text{heatmap}(t) = \alpha \cdot \text{heatmap}(t - 1) + \Delta H(t) \tag{28}$$

where $\Delta H(t)$ is the heat increment contributed by vehicles in frame t.

3. Calculating Lane Utilization Rate

For the emergency lane R_3, the total heat is given by Equation (29).

$$H_3 = \sum_{(x,y) \in R_3} \text{heatmap}(x, y) \tag{29}$$

The lane utilization rate is defined as the ratio of the current total heat to the maximum total heat, as shown in Equation (30).

$$U_3 = \frac{H_3}{H_{\text{max},3}} \tag{30}$$

By calculating U_3, we can reflect the utilization level of the emergency lane, further improving the basis for activating the emergency lane. If the utilization level of the emergency lane is low after being open for a period, closing the emergency lane can be considered. Therefore, by using U_i as an important basis for closing the emergency lane, the final emergency lane activation flowchart is shown in Figure 21.
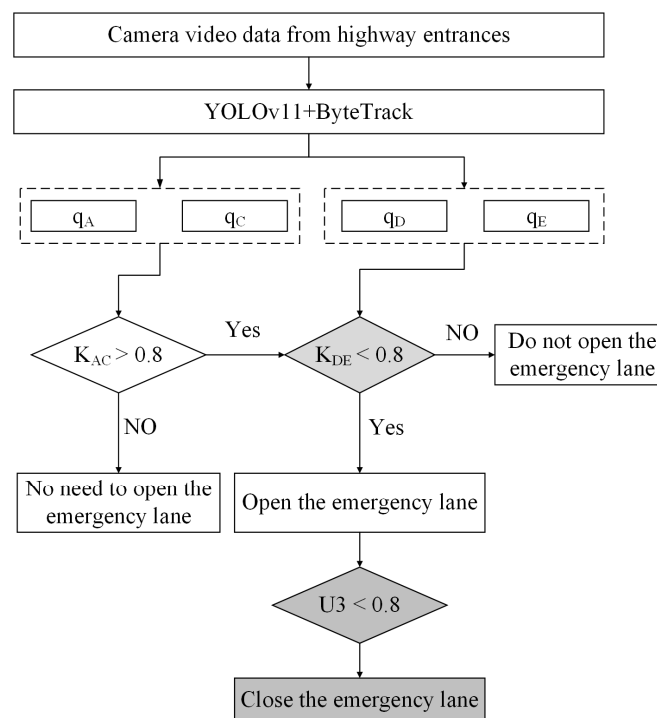
Figure 21. Emergency lane activation/closure decision flowchart (after adding point F within the CD interval).

6. Limitations

However, it should be noted that the quantitative analysis of the benefits of emergency lane activation above is based on the following three important assumptions:

1. Assumption of Traffic Capacity Improvement: It is assumed that after activating the emergency lane, the traffic capacity increases by 30%; the actual improvement range needs to be determined according to specific road conditions and traffic management measures.

2. Linear Relationship of Flow Rate Changes: It is assumed that the downstream flow rate $q_D(t)$ increases by 30%, without considering the impact of traffic behavior and driver response factors.

3. Applicability of the Occupancy Rate Model: The model does not consider the impact of other external factors (such as weather, accidents, etc.) on the traffic flow.

Additionally, it should be noted that this method has a specific application domain: it is most suitable for highways with limited intersections. When considering urban areas with numerous intersections and complex road networks, two primary limitations emerge: (1) The interval definition becomes significantly more complex due to multiple entry and exit points within a given section; (2) The high density of intersections substantially increases the complexity of real-time decision-making, as traffic flow patterns become more intricate with vehicles entering and exiting at multiple points. Addressing these urban-specific challenges would require more rigorous design protocols and sophisticated modeling approaches that can account for the complex dynamics of urban traffic networks.

7. Conclusions

The traffic congestion prediction and emergency lane development strategy based on the object detection algorithms proposed in this paper achieves the scientific activation and closure of emergency lanes through effective model construction and optimized layouts, thereby enhancing traffic management efficiency and road capacity. The main conclusions are as follows:

1. Real-Time Traffic Flow Parameter Extraction and Prediction: By utilizing YOLOv11 and ByteTrack algorithms, real-time traffic flow data (flow rate, speed, density) extraction at

four monitoring points was successfully achieved. Combined with the AdaBoost regression model, downstream traffic density can be predicted in advance, providing data support for the activation of emergency lanes.

2. Effective Application of the Interval Occupancy Rate Model: Based on the interval occupancy rate model, this paper analyzed the causes of congestion in the CD interval and determined the formation mechanism of traffic congestion when the vehicle occupancy rate $K_{CD}(t)$ exceeded 80%. The model's real-time calculations then guided the activation and closure of emergency lanes.

3. Quantitative Analysis of the Benefits of Emergency Lane Activation: After activating the emergency lane, the congestion duration was reduced by 48.3%, and the peak occupancy rate of congestion decreased to 0.917, significantly improving the traffic capacity of the CD section, alleviating traffic congestion, and shortening the congestion duration.

4. Optimization Suggestions for Monitoring Point Layout: By adding monitoring point F within the CD interval and establishing a lane utilization rate model, the precision and rationality of emergency lane management were further enhanced. Additionally, adjusting the monitoring point layout can be considered to minimize costs while ensuring effective coverage of the monitoring range.

Institutional Review Board Statement: Not applicable.

Informed Consent Statement: Not applicable.

Data Availability Statement: The datasets used and analyzed during the current study are available from the corresponding author on reasonable request.

Conflicts of Interest: The authors declare no conflicts of interest.

References

1. Wang, S.; Djahel, S.; Zhang, Z.; McManis, J. Next Road Rerouting: A Multiagent System for Mitigating Unexpected Urban Traffic Congestion. *IEEE Trans. Intell. Transp. Syst.* **2016**, *17*, 2888–2899. [CrossRef]
2. Jiang, P.; Liu, L.; Cui, L.; Li, H.; Shi, Y. Congestion Prediction of Urban Traffic Employing SRBDP. In Proceedings of the 2017 IEEE International Symposium on Parallel and Distributed Processing with Applications and 2017 IEEE International Conference on Ubiquitous Computing and Communications (ISPA/IUCC), Guangzhou, China, 12–15 December 2017; pp. 1099–1106.
3. Bista, R.B.; Paneru, S. Does Road Traffic Congestion Increase Fuel Consumption of Households in Kathmandu City? *J. Econ. Impact* **2021**, *3*, 67–79. [CrossRef]
4. Rahman, M.M.; Najaf, P.; Fields, M.G.; Thill, J.-C. Traffic Congestion and Its Urban Scale Factors: Empirical Evidence from American Urban Areas. *Int. J. Sustain. Transp.* **2022**, *16*, 406–421. [CrossRef]
5. Yang, Y.; Liu, Q.; Shi, Y. Study on Decision Model of Dynamic Hard Shoulder Running for Highways with Saturated Traffic Volume. *Highw. Eng.* **2022**, *47*, 172–176. [CrossRef]
6. Khatri, A.; Senthilkumar, M. Lane Clearance Approach for Emergency Vehicles in Highways Network. *PLoS ONE* **2022**, *17*, e0276988. [CrossRef]
7. Yang, F.; Wang, F.; Ding, F.; Tan, H.; Ran, B. Identify Optimal Traffic Condition and Speed Limit for Hard Shoulder Running Strategy. *Sustainability* **2021**, *13*, 1822. [CrossRef]
8. Huang, Z.; Loo, B.P.Y. Urban Traffic Congestion in Twelve Large Metropolitan Cities: A Thematic Analysis of Local News Contents, 2009–2018. *Int. J. Sustain. Transp.* **2023**, *17*, 592–614. [CrossRef]
9. Li, G.; Wang, Q.; Zuo, C. Emergency Lane Vehicle Detection and Classification Method Based on Logistic Regression and a Deep Convolutional Network. *Neural Comput. Appl.* **2022**, *34*, 12517–12526. [CrossRef]
10. Bai, M.; Lin, Y.; Ma, M.; Wang, P. Travel-Time Prediction Methods: A Review. In *Smart Computing and Communication*; Qiu, M., Ed.; Springer International Publishing: Cham, Switzerland, 2018; pp. 67–77.

11. Ben-Akiva, M.; Bierlaire, M.; Burton, D.; Koutsopoulos, H.N.; Mishalani, R. Network State Estimation and Prediction for Real-Time Traffic Management. *Netw. Spat. Econ.* **2001**, *1*, 293–318. [CrossRef]

12. Skabardonis, A.; Geroliminis, N. Real-Time Estimation of Travel Times on Signalized Arterials. In *Transportation and Traffic Theory: Flow, Dynamics and Human Interaction*; Elsevier: Amsterdam, The Netherlands, 2005; pp. 387–406.

13. Nanthawichit, C.; Nakatsuji, T.; Suzuki, H. Application of Probe-Vehicle Data for Real-Time Traffic-State Estimation and Short-Term Travel-Time Prediction on a Freeway. *Transp. Res. Rec.* **2003**, *1855*, 49–59. [CrossRef]

14. Zhang, X.; Rice, J.A. Short-Term Travel Time Prediction. *Transp. Res. Part C Emerg. Technol.* **2003**, *11*, 187–210. [CrossRef]

15. Onyeneke, C.; Eguzouwa, C.; Mutabazi, C. Modeling the Effects of Traffic Congestion on Economic Activities—Accidents, Fatalities and Casualties. *Biomed. Stat. Inform.* **2018**, *3*, 7–14. [CrossRef]

16. Salamanis, A.; Kehagias, D.D.; Filelis-Papadopoulos, C.K.; Tzovaras, D.; Gravvanis, G.A. Managing Spatial Graph Dependencies in Large Volumes of Traffic Data for Travel-Time Prediction. *IEEE Trans. Intell. Transp. Syst.* **2016**, *17*, 1678–1687. [CrossRef]

17. Achar, A.; Bharathi, D.; Kumar, B.A.; Vanajakshi, L. Bus Arrival Time Prediction: A Spatial Kalman Filter Approach. *IEEE Trans. Intell. Transp. Syst.* **2020**, *21*, 1298–1307. [CrossRef]

18. Zhang, L.; Ma, J.; Zhu, C. Theory Modeling and Application of an Adaptive Kalman Filter for Short-Term Traffic Flow Prediction. *J. Inf. Comput. Sci.* **2012**, *9*, 5101–5109.

19. Fei, X.; Lu, C.-C.; Liu, K. A Bayesian Dynamic Linear Model Approach for Real-Time Short-Term Freeway Travel Time Prediction. *Transp. Res. Part C Emerg. Technol.* **2011**, *19*, 1306–1318. [CrossRef]

20. Chen, Z.; Jiang, Y.; Sun, D. Discrimination and Prediction of Traffic Congestion States of Urban Road Network Based on Spatio-Temporal Correlation. *IEEE Access* **2020**, *8*, 3330–3342. [CrossRef]

21. Maulida, N.R.; Mutijarsa, K. Traffic Density Classification Using Multilayer Perceptron and Random Forest Method. In Proceedings of the 2021 International Seminar on Intelligent Technology and Its Applications (ISITIA), Surabaya, Indonesia, 21–22 July 2021; pp. 117–122.

22. Jiang, Q.; Liao, X.; Gong, Y.; Ma, J. An Attention-Based Multi-Context Convolutional Encoder-Decoder Neural Network for Work Zone Traffic Impact Prediction. *arXiv* **2024**, arXiv:2405.21045.

23. Wang, L.; Che, L.; Lam, K.-Y.; Liu, W.; Li, F. Mobile Traffic Prediction with Attention-Based Hybrid Deep Learning. *Phys. Commun.* **2024**, *66*, 102420. [CrossRef]

24. Zechin, D.; Cybis, H.B.B. Probabilistic Traffic Breakdown Forecasting through Bayesian Approximation Using Variational LSTMs. *Transp. B Transp. Dyn.* **2023**, *11*, 1026–1044. [CrossRef]

25. Zhang, T.; Wang, J.; Wang, T.; Pang, Y.; Wang, P.; Wang, W. A Deep Marked Graph Process Model for Citywide Traffic Congestion Forecasting. *Comput.-Aided Civ. Infrastruct. Eng.* **2024**, *39*, 1180–1196. [CrossRef]

26. Gao, H.; Jia, H.; Yang, L. An Improved CEEMDAN-FE-TCN Model for Highway Traffic Flow Prediction. *J. Adv. Transp.* **2022**, *2022*, 2265000. [CrossRef]

27. Li, W.; Liu, X.; Tao, W.; Zhang, L.; Zou, J.; Pan, Y.; Pan, Z. Location and Time Embedded Feature Representation for Spatiotemporal Traffic Prediction. *Expert Syst. Appl.* **2024**, *239*, 122449. [CrossRef]

28. Jin, S.; Lee, H.; Park, C.; Chu, H.; Tae, Y.; Choo, J.; Ko, S. A Visual Analytics System for Improving Attention-Based Traffic Forecasting Models. *IEEE Trans. Vis. Comput. Graph.* **2023**, *29*, 1102–1112. [CrossRef] [PubMed]

29. Ei Leen, M.W.; Jafry, N.H.A.; Salleh, N.M.; Hwang, H.; Jalil, N.A. Mitigating Traffic Congestion in Smart and Sustainable Cities Using Machine Learning: A Review. In *Proceedings of the Computational Science and Its Applications—ICCSA 2023*; Gervasi, O., Murgante, B., Taniar, D., Apduhan, B.O., Braga, A.C., Garau, C., Stratigea, A., Eds.; Springer Nature: Cham, Switzerland, 2023; pp. 321–331.

30. Modi, Y.; Teli, R.; Mehta, A.; Shah, K.; Shah, M. A Comprehensive Review on Intelligent Traffic Management Using Machine Learning Algorithms. *Innov. Infrastruct. Solut.* **2021**, *7*, 128. [CrossRef]

31. Behrooz, H.; Hayeri, Y.M. Machine Learning Applications in Surface Transportation Systems: A Literature Review. *Appl. Sci.* **2022**, *12*, 9156. [CrossRef]

32. Szele, A.; Kisgyörgy, L. Traffic Management of the Congested Urban-Suburban Arterial Roads. *Period. Polytech. Civ. Eng.* **2019**, *63*, 1103–1111. [CrossRef]

33. Guide, T.M. *Traffic Monitoring Guide*; Federal Highway Administration: Washington, DC, USA, 2001.

34. Girshick, R.; Donahue, J.; Darrell, T.; Malik, J. Rich Feature Hierarchies for Accurate Object Detection and Semantic Segmentation. In Proceedings of the Proceedings of the IEEE Conference on Computer Vision and Pattern Recognition (CVPR), Columbus, OH, USA, 23–28 June 2014; pp. 580–587.

35. Girshick, R. Fast R-CNN. *arXiv* **2015**, arXiv:1504.08083.

36. Ren, S.; He, K.; Girshick, R.; Sun, J. Faster R-CNN: Towards Real-Time Object Detection with Region Proposal Networks. In *Advances in Neural Information Processing Systems*; Curran Associates, Inc.: Red Hook, NY, USA, 2015; Volume 28.

37. Kim, B.; Natarajan, Y.; Preethaa, K.R.S.; Song, S.; An, J.; Mohan, S. Real-Time Assessment of Surface Cracks in Concrete Structures Using Integrated Deep Neural Networks with Autonomous Unmanned Aerial Vehicle. *Eng. Appl. Artif. Intell.* **2024**, *129*, 107537. [CrossRef]

38. Redmon, J.; Divvala, S.; Girshick, R.; Farhadi, A. You Only Look Once: Unified, Real-Time Object Detection. In Proceedings of the 2016 IEEE Conference on Computer Vision and Pattern Recognition (CVPR), Las Vegas, NV, USA, 27–30 June 2016; pp. 779–788.

39. Liu, W.; Anguelov, D.; Erhan, D.; Szegedy, C.; Reed, S.; Fu, C.-Y.; Berg, A.C. SSD: Single Shot MultiBox Detector. In *Proceedings of the Computer Vision—ECCV 2016*; Leibe, B., Matas, J., Sebe, N., Welling, M., Eds.; Springer International Publishing: Cham, Switzerland, 2016; Volume 9905, pp. 21–37.

40. Guo, S.; Li, S.; Han, Z.; Gao, M.; Wang, Z.; Li, H. Efficient Detection of Multiscale Defects on Metal Surfaces with Improved YOLOv5. *Multimed. Tools Appl.* **2024**, *83*, 85253–85275. [CrossRef]

41. Ultralytics New Yolo11. Available online: https://docs.ultralytics.com/models/yolo11 (accessed on 3 October 2024).

42. Li, Z.; He, Q.; Yang, W. E-FPN: An Enhanced Feature Pyramid Network for UAV Scenarios Detection. *Vis. Comput.* **2024**, 1–19. [CrossRef]

43. Zhu, X.; Lyu, S.; Wang, X.; Zhao, Q. TPH-YOLOv5: Improved YOLOv5 Based on Transformer Prediction Head for Object Detection on Drone-Captured Scenarios. In Proceedings of the 2021 IEEE/CVF International Conference on Computer Vision Workshops (ICCVW), Montreal, BC, Canada, 11–17 October 2021; p. 2788.

44. Zhang, Y.; Sun, P.; Jiang, Y.; Yu, D.; Weng, F.; Yuan, Z.; Luo, P.; Liu, W.; Wang, X. ByteTrack: Multi-Object Tracking by Associating Every Detection Box. In *European Conference on Computer Vision*; Springer Nature: Cham, Switzerland, 2022.

45. Kuhn, H.W. The Hungarian Method for the Assignment Problem. *Nav. Res. Logist. Q.* **1955**, *2*, 83–97. [CrossRef]

46. Zhi, N.; An, Y.; Zhao, Y.; Qiu, J. Intelligent Island Detection Method of DC Microgrid Based on Adaboost Algorithm. *Energy Rep.* **2023**, *9*, 970–982. [CrossRef]

47. Miller, K. Boosting Algorithm in Python. Available online: https://python-course.eu/machine-learning/boosting-algorithm-in-python.php (accessed on 26 September 2024).